Mechanical model to evaluate steel reinforcement corrosion effects on σ-ε and fatigue curves. Experimental calibration and validation.

Ignasi Fernandez*[1], Jesús Miguel Bairán[1], Antonio R. Marí[1]

[1] Department of Construction Engineering, Polytechnic University of Catalonia, Jordi Girona, 1-3, Barcelona 08034, Spain.

*corresponding author: ignasi.fernandez@chalmers.se

Highlights:

- Mechanical model to evaluate the mechanical properties of corroded steel
- Calibration and validation of a mechanical model to evaluate corrosion effect on tensile and fatigue curves
- An experimental study on material properties characterization for not corroded bars produced with TEMPCORE® system.
- Experimental data validates the presented model from 0% up to 60% degree of corrosion.

Abstract:

An experimental study to characterize the annular distribution of the mechanical properties throughout the cross-section of TEMPCORE® steel bars is presented. Thereafter a sectional fibre model, which allows obtaining σ-ε and fatigue curves of corroded steel, is described. The model is calibrated using an extensive experimental study of artificially corroded steel bars tested under cyclic and monotonic loads. Local pitting effects such as stress concentration, local bending or non-uniform material properties distribution are considered. Validation of the model is done

using different experimental work in the literature, which encompassed naturally and artificially corroded bars, for both fatigue and monotonic tests.

Keywords: steel reinforced concrete; mass loss; pitting corrosion; modelling studies

1. Introduction

The study of corrosion effects is crucial for a better understanding of the structural behaviour of existing impaired concrete structures and, therefore, for their durability assessment. Effects such as the loss of bond between concrete and steel reinforcement, reduction of steel cross-section or concrete longitudinal cracking due to rust expansiveness, which leads to splitting stresses on the surrounding concrete, have been widely studied [1–4]. However, other local corrosion effects that lead to a steel mechanical behaviour changes [5–11] are relevant too. Both pitting and generalized corrosion of steel reinforcement bars lead to a change in the cross-section geometry. These changes turn into local effects in steel cross-section such as non-uniform stress distribution due to both stress localization in the top of the pits and local bending due to the centre of gravity displacement.

On the other hand some modern production systems, such as TEMPCORE® production system, produces a heterogeneous material properties throughout the steel cross-section; being the apparent σ-ε characterization of the bar, the mean response of the heterogeneous section. Specifically annular distribution of the mechanical properties is defined for this steel manufacture system [6,12–18], in which the outer layers resist more than the inner core. Consequently, due to the non-uniform cross-section reduction of steel corrosion, the non-uniform stress throughout the cross-section and the reduction of the bar capacity are emphasised.

In this work, an experimental study to define a realistic material distribution throughout the steel cross-section was performed. Different specimens with reduced cross-section diameters were tested using monotonic loads. After post-processing the experimental data, it was possible to

define the mechanical properties throughout the cross-section, i.e. the annular distribution of the yielding and ultimate stresses.

Thereafter, a mechanical model to evaluate steel reinforcement corrosion effects on σ-ε and fatigue curves is presented. The model takes into account the reduction of cross-section either generalized or localized due to pitting corrosion. Pitting corrosion is considered by means of a notch in the cross-section, associated with a degree of corrosion. Generalized corrosion is taken into account by means of the critical cross-section definition, in which a double steel cross-section reduction is performed; a reduction due to the corrosion penetration (generalized corrosion) besides a notch. In both cases, notches are described as perfect ellipses, further details are provided.

On the other hand, material heterogeneity in the cross sections due to current production systems of reinforcing bars such as TEMPCORE® is considered by discretizing the cross-section in two different layers. The damage produced by load cycles is defined in accordance with the Palmgren-Miner damage law [19,20], by which fatigue curves for corroded steel bars can be obtained

A statistical model relating the pit geometry with the degree of corrosion was developed and calibrated using different experimental data found in the literature [21], which essentially encompassed artificially corroded steel bars tested under cyclic and monotonic loads. Thereafter, the mechanical model was validated by means of monotonic and fatigue tests of artificially and naturally corroded steel bars [8,21,22].

2. Material behaviour. TEMPCORE® steel reinforcement bars.

An experimental study was conducted in order to define the mechanical properties of uncorroded heterogeneous steel reinforcement bars. TEMPCORE® production system consists of the application of cold water after the steel conformation with the purpose to decrease quickly its temperature. The temperature of the water and the applied time defines the steel microstructure and thereafter the final mechanical properties. The common microstructure obtained is a ferrite core followed by a mix ferrite-martensitic (or bainitic transition crown which is the responsible of the smooth changes in the stresses between microstructures, see Figure 3a [18]) and finally, an outer martensitic layer. The aim of the presented experimental study was the characterization of the mechanical properties of 12 mm diameter steel bars used for the calibration and validation of the given model.

2.1 Test setup

The tests aimed the characterization of the tensile mechanical steel properties distribution throughout the cross-section. By performing monotonic tests to uncorroded specimens with different cross-section reductions, the different σ-ε curves were obtained (see Figure 1a). The reduction of cross-section was performed using a milling machine. Different crown thicknesses were removed from each specimen using a diamond tip. The actual diameter was checked using a Vernier calliper to know the exact remaining cylindrical steel area.

Figure 1. a) Reduced cross-section specimens. b) INSTRON 8800 transducer

Tests were performed following the standard [23]. The specimens were afixed to the clamps, and the load was directly applied to the bar via a hydraulic jack controlled with a load cell placed on the top. The same jack had an active displacement control system so the tests could be controlled by the total applied displacement. A 50 mm displacement transducer was placed at the reduced cross-section zone in order to register the real strain of the bar, avoiding machine deformations, slip in the clamps and complete cross-section bar deformation. All the tested specimens failed in the middle of the reduced cross-section zone. Member length between clamps was 110 mm, and the reduced cross-section length was 70 mm, enough to assure uniform stress distribution. Monotonic tests were carried out by means of a test machine INSTRON 8803, see Figure 1b. The diameters tested are described in Table 1.

Table 1. Tested diameter for material characterization

Steel reduced diameter [mm]
6
8
9
10
11/11.5 (only removing ribs)
Theoretical 12 (whole section)

2.2 Results of monotonic test

σ-ε curves of tested members with reduced diameter are presented in Figure 2. The strains described, corresponded to the ones recorded by the displacement transducer (50 mm range) placed on the bars. The stresses depicted in the figures resulted from the division of the recorded load by the steel reduced area, (measuring the corroded diameter with the calliper).

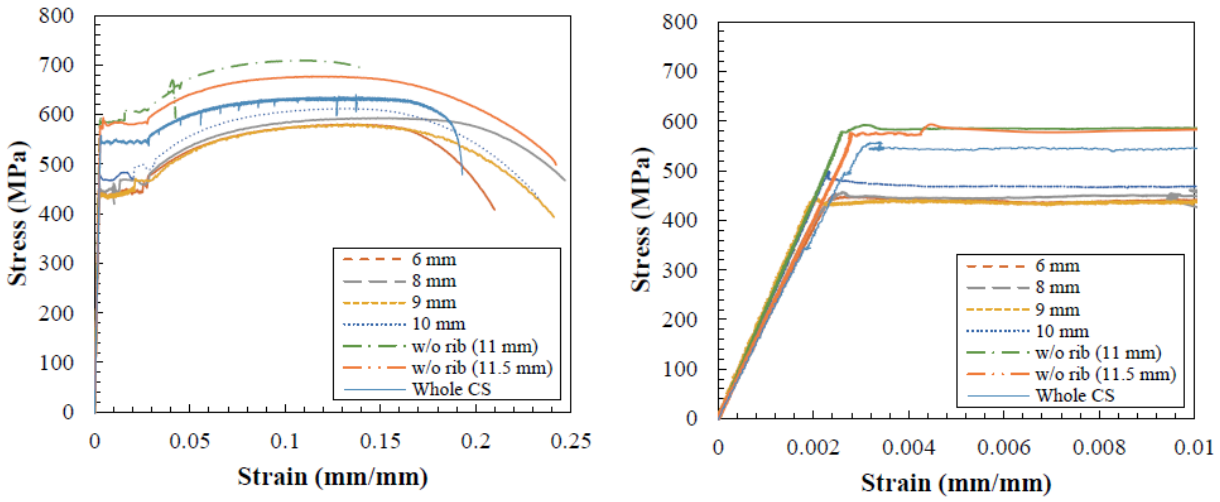

Figure 2. σ-ε of reduced cross-section a) up to failure b) up to the elastic limit.

All the curves presented in Figure 2 corresponded to the mean value between the ferrite core and the adjacent martensitic layers. A post-processing of the experimental data to obtain the real

material properties of the layer itself was performed. Different specimens were tested to obtain the diameter of the ferrite core. From that, successive crowns of 0.5 mm thickness were added until the complete steel bar was tested, see Figure 3b.

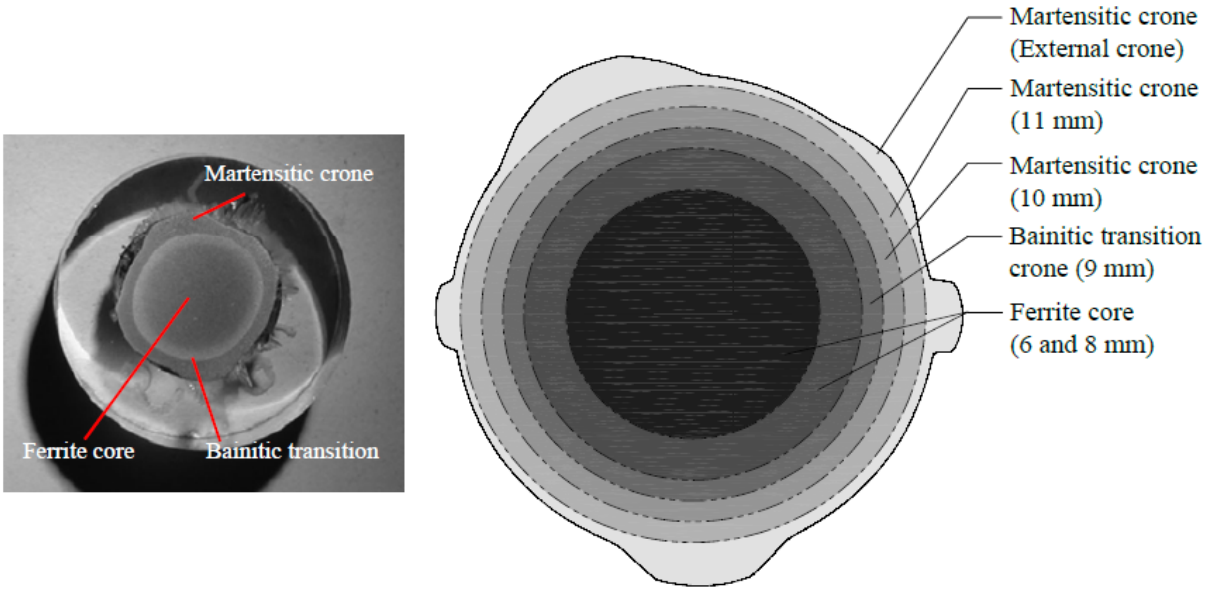

Figure 3. a) Real 16 mm diameter bar [18]. b) Ferrite core, bainitic transition and martensitic crowns up to whole cross-section

Table 2. Real elastic limits and ultimate strength obtained after experimental data post-processing

Specimens (12 mm diameter)	External radius (mm)	fy (MPa)	fu (MPa)
Ferrite core	4	435	575
Crown 1 (Ferrite)	4.25	522	601
Crown 2	4.5	583	642
Crown 3	4.75	655	682
Crown 4	5	705	718
Crown 5	5.25	749	757
Crown 6	5.5	783	789
Crown 7	5.75	806	824
Outer crown	6	806	824

Applying the product-summation series described in Eq. 1 the material properties for each particular crown could be obtained. The final elastic limit and ultimate strength values for the different layers are shown in Table 2.

(1) $\sum A_i \cdot f_{y_i} = \overline{A} \cdot \overline{f_y}$

The final profile of the elastic limit and ultimate strength along the cross-section is described in Figure 4a, and the idealized σ-ε curve for each crown is described in Figure 4b.

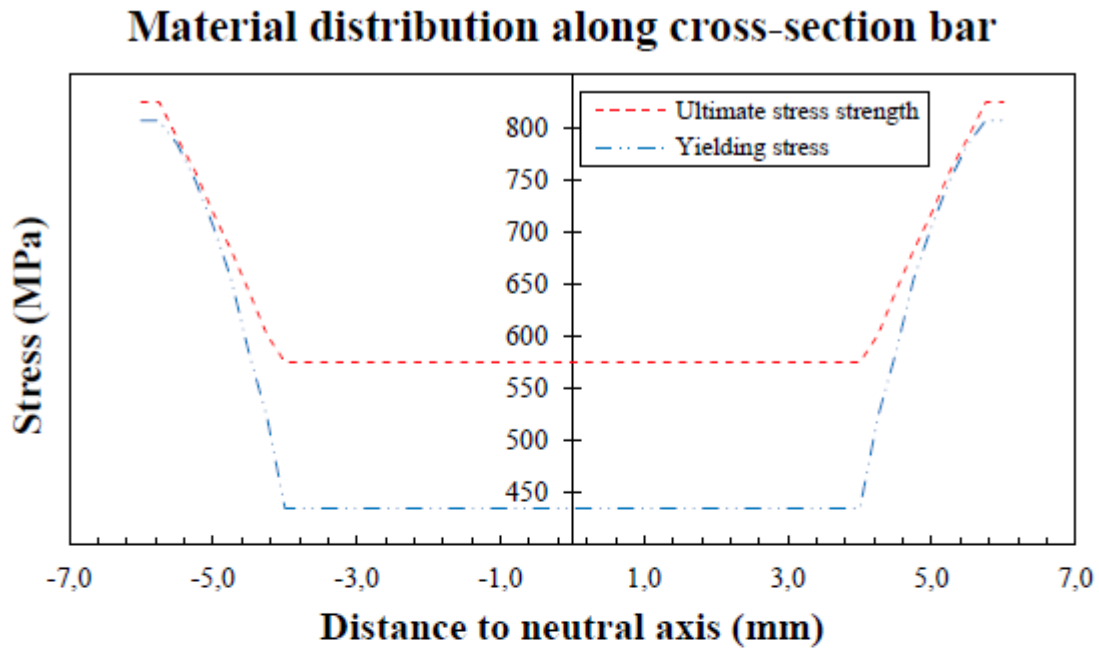

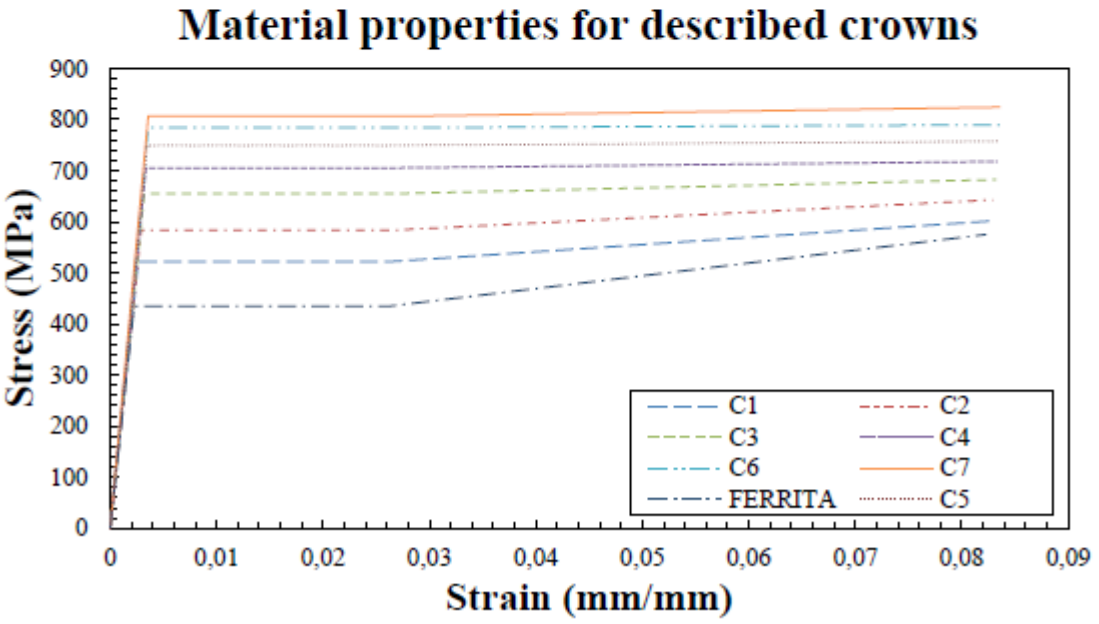

Figure 4. a) Obtained stress profile from the tested bars. b) σ-ε final curves of each discretized layer

119

The measured capacity of the specimens, on which only the ribs were removed, resulted higher than that of measured considering the whole bar. The influence of the ribs in the sectional behaviour resulted in a reduction of the mechanical properties. This phenomenon was due to 3D stress effects produced by the ribs, since they did not contribute as much as the other parts of the r section to the bar carrying capacity, see Figure 5.

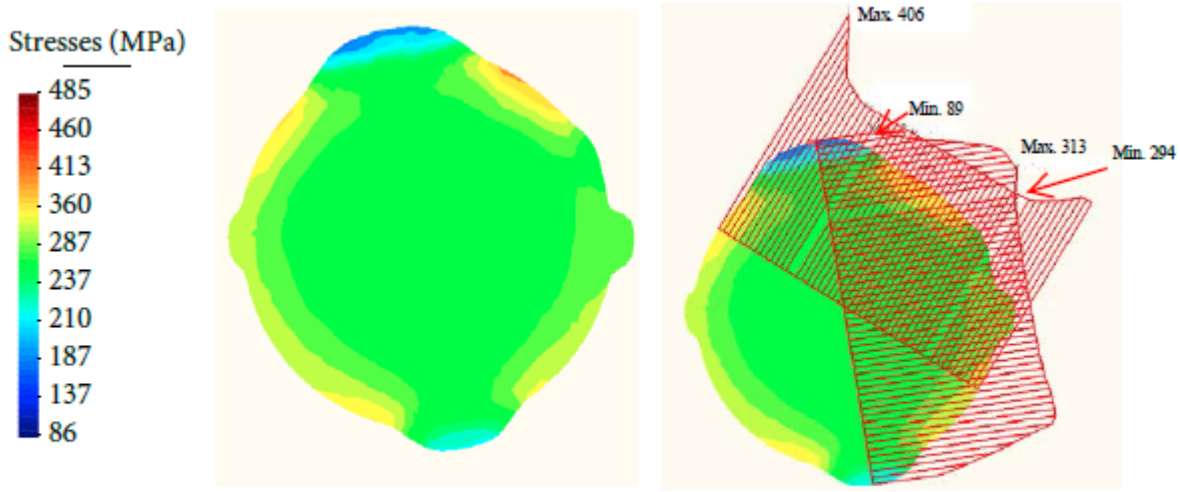

Figure 5. Geometric effect of ribs (bar cross-section) diametrical stress profiles

3. Description of the mechanical model

3.1 Material model

After the presented experimental study and taking into account the results obtained by Bairán et al. [13] a simplified bi-layer material model was chosen; an inner ferrite core and an outer martensitic crown, which described the average behaviour for all the remaining layers, see Figure 6. The inner core diameter was calibrated by means of the experimental data presented before.

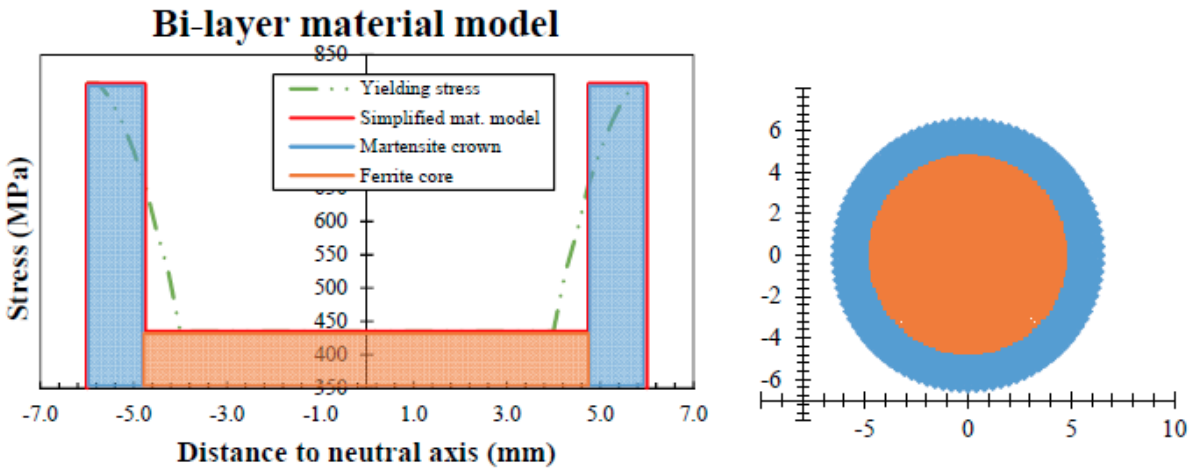

Figure 6. Simplified by-layer material model used in this work. Inner ferrite core; outer martensitic crown

132

133 *3.2 Cross-section definition and constitutive equation*

134 The model uses a fibre discretization of the steel reinforcement cross-section in order to
135 incorporate the variety of mechanical properties throughout it. This approach can accurately
136 describe the bar geometry as well as the material heterogeneity. This work is focused on this
137 manufacturing process as far as it is the most extended production system for steel reinforcement
138 bars in Europe.

139 The behaviour under large cyclic loading histories was controlled using material's hardening
140 rules. The steel proposed material model is a mix of the two existing models in the literature:
141 kinematic an isotropic hardening. Therefore, the mixed-hardening model developed by Bairan et
142 al. [16] was implemented in the present mechanical model.

143 *3.3 Implementation of steel corrosion*

144 Both generalised corrosion and pitting corrosion of reinforcement steel bars were considered in
145 the presented model. The weakest section of the bar, where most likely it would fail (Figure 7a),
146 is defined. , This section is was represented as a circular cross-section with a unique equivalent

147 pit (circular idealized cross-section, see Figure 7b). Both generalized and pitting corrosion could
148 be simulated considering this critical circular pitted cross-section.

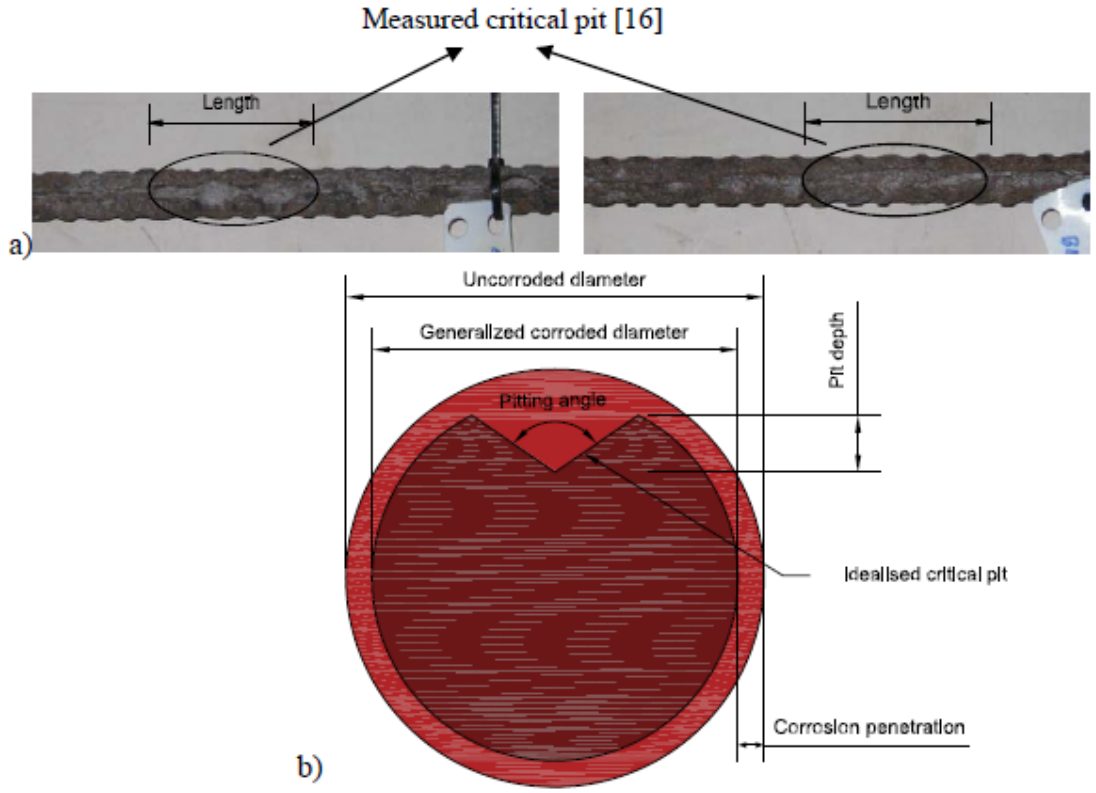

Figure 7. a) Measured pit in the critical cross-section. b) Pitting and generalised corrosion implementation

149

150 By defining a pit, which includes the steel cross-section reduction due to corrosion penetration,
151 the pitting corrosion was implemented. On the other hand, a double cross-section reduction to
152 reproduce generalized corrosion phenomenon was performed on the uncorroded idealised cross-
153 section; first, a corrosion penetration due to the estimated corrosion degree (generalised
154 corrosion) was applied, see Figure 7b. This reduction led to a new smaller circular idealized
155 diameter, $\phi_{cor} < \phi$. Thereafter, a pit was performed to that new reduced cross-section, which
156 geometrical specs depended on the estimated degree of corrosion and were calibrated by means

of the statistical model presented below using experimental tests. This implementation responds to the observed pit distribution along the specimens even though uniform corrosion.

A half ellipse hypothesis, defined by its major and minor axes, to reproduce the geometrical shape of the pit was idealized. Depth, length and angle in the section plane defined the main geometrical parameters of the pit. The critical cross-section was placed in the maximum depth of the ellipse, minor axis, whereas the major axis represented the pit length in the longitudinal direction bar, see Figure 7a and Figure 8.

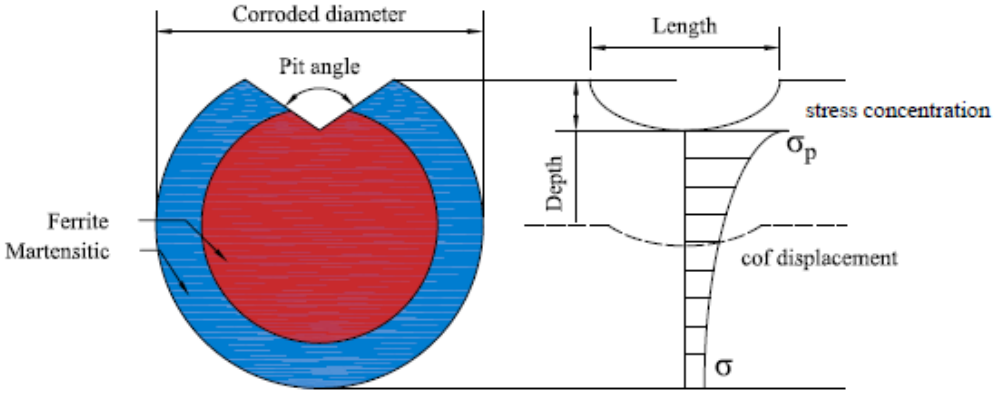

Figure 8. Pit effect in the steel cross-section: stress localization and local bending moment. Pitt definition in the model

Localization stresses factor over the notch tip, and linear fracture mechanics criteria [24] were applied thanks to the ellipse hypothesis. Eq. 2 defined the stress at the notch tip (σ_p), where σ_n was the pressure under plain strain distribution hypothesis. L and p were the pit length and depth respectively (see Figure 7 and Figure 8). Stress amplification in the different points of the cross-section was a function of the distance to the notch tip, and it followed the Airy function [24].

(2) $$\sigma_p = \sigma_n(1 + \frac{4p}{L})$$

Because the assumptions made, the model allows the application of any stress and temperature histories to the bar. A monotonic load was applied by means of strain control. Fatigue test was a particular case in which a desired load history was applied. History of stresses or local yielding was possible to be simulated.

3.4 Fatigue model description

Fatigue analyses were performed using a specific stress range, which was referred to the whole cross-section (using uncorroded nominal diameter and circular idealised cross-section hypothesis). Raw materials were considered, i.e. the variation of the mechanical properties due to corrosion was not considered in fatigue analysis. The maximum and the minimum stresses at every fibre in the cross-section were determined after each analysis. Then, the number of resisted cycles of each fibre submitted to the defined stress range could be obtained.

By modifying the number of cycles resisted by each fibre, the effect of the applied mean stress was considered, i.e. two fibres subjected to the same stress range resisted different number of cycles depending on the applied σ_m value. In addition, the reduction of the resisted cycles with the temperature, was also considered.

Palmgren-Miner, Eq. 3, was used to define the damage state of each fibre after every load step (i).

(3) $d_i = \frac{n_i}{N_i}$

Where N was the cycle resisted number, n the number of times the applied stress range was and d the fibre damage state index. The damage was accumulated during every load step. When the fibre achieved damage index 1, it was considered broken, and it was removed from the cross-

191 section for the next steps iteratively until the last group of fibres did not resist the applied stress
192 range. Thereafter the cycle resisted number, N, was stated as the fatigue life value.

193 **4. Model calibration**

194 *4.1 Experimental data for the model calibration*

195 An extensive database of corroded reinforcing steel bars submitted to monotonic and cycle
196 loading [21] were used for calibration purposes. That work focused on direct monotonic and
197 cyclic tests of corroded reinforcement bars extracted from statically undetermined beams exposed
198 to accelerated corrosion with different degrees of corrosion [25], see Figure 9.

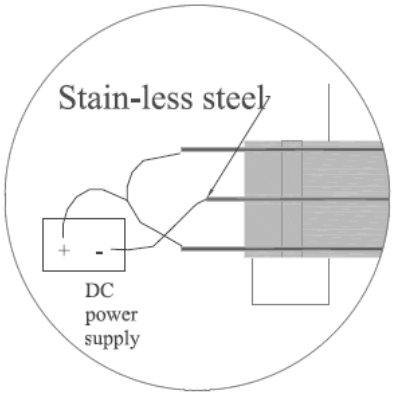

199 **Figure 9. Connection scheme for the impressed corrosion**

200 *4.2 Accelerated corrosion*

201 The experimental work used for calibration purposes encompassed more than 180 specimens
202 submitted to accelerated corrosion and thereafter tested under monotonic and cyclic loads.

203 Accelerated corrosion methods open the possibility to reproduce corrosion episodes over
204 structures in very short periods, as compared to natural corrosion. Those methods has been used
205 extensively in the literature [26–30]. Obviously, this form of corrosion mechanism has some

drawbacks compared to natural corrosion testing. Further, the corrosion procedure for accelerated corrosion method resulted in homogeneous corrosion along the bar, by means of pits distributed along the steel specimen. They are nevertheless necessary to investigate the effects on structures and materials over time within an appropriate investigation period. With this kind of methods, it is possible to reproduce a 20-30 years' phenomenon in a few months with a reasonable agreement between the natural and induced corrosion effects.

4.2.1 Corrosion method

Corrosion of steel reinforcement was forced using current galvanostatic method. A DC power supply was used for applying a constant current to the different members. The current was constant during all the exposure time. The steel bar was connected to the positive pole of the power supply, used as an anode, meanwhile the stain-less steel bar used as cathode was connected to the negative pole.

Following Faraday's law Eq. 4, it was possible to estimate the mass loss of steel due to corrosion, knowing the applied intensity along time, I(t), and the geometrical bar properties such as diameter and exposed length.

Eq. 4 $$E = \frac{m_{Fe} \cdot \int I \cdot dt}{z \cdot F}$$

In Eq. 4 Fe is the atomic mass, z is the steel valence that is taken as equal to two and F is Faraday's constant. As the applied intensity was an input during the test and it is also constant along time, it is possible to rewrite Faraday's law as Eq. 5

Eq 5 $$\Delta m = \frac{m_{Fe} \cdot I \cdot t}{z \cdot F}$$

Many researchers have observed [31,32] that, using corrosion current densities below 350 $\mu A/cm^2$ for accelerated corrosion, the difference between the corrosion rate estimated by means of Faraday's law and the corrosion rate registered from gravimetric methods (steel weight measure after accelerated corrosion) ranges between 5-10%. Thus, by applying corrosion current density values below this threshold, it is possible to accurately estimate the achieved degree of corrosion. Furthermore, current densities above this threshold imply moving the test further away from a natural corrosion process. In the presented work, corrosion rates below 350 $\mu A/cm^2$ were applied here in order to corrode the specimens.

Accelerated corrosion methods based on impressed current need depassivated steel for proper development. This means that it is necessary to previously depassivate steel bars. In the aforementioned study a 4% sodium chloride (NaCl) solution in the water used for concrete casting was chosen in order to eliminate the passive layer by means of chloride attack. Further details of the corrosion method and the corrosion procedure are described in Fernandez et al. [25].

After the time exposure was reached the beams were crushed and the reinforcement steel bars extracted. Following the code recommendations [33] the specimens were cleaned. Thereafter by means of mass loss determination each specimen degree of corrosion or generalized degree of corrosion was determined. The described degree of corrosion was used for the model calibration described below.

4.3 Specimen and test description

The specimens employed for monotonic testing had in between 310 mm and 320 mm length. The ends of the test specimen were affixed by two clamps, which were used to transfer directly the

load to the specimen. The tested free section was for all the specimens 170 mm letting 70/75 mm length for each clamp. Tests were conducted by means of displacement control. Uncorroded specimens also were tested to compare and assess the influence of degree of corrosion on the mechanical properties. In total 40 specimens were tested satisfactorily with a range of degrees of corrosion between 8% and 22%.

Fatigue test specimens also had in between 310 mm and 320 mm length. The ends of the test specimen were affixed by two clamps, which were used to transfer directly the load to the specimen. The tested free length was for all the specimens 170 mm letting 70/75 mm length for each clamp. In that case, tests were conducted using load control.

Three different stress ranges were defined for fatigue tests, 150 MPa, 200 MPa and 300 MPa ($\Delta S=S_{max} - S_{min}$). The minimum stress ($S_{min}$) was defined avoiding compressions in the bar and its possible buckling effects. The maximum stress (S_{max}) was lower than $0.6*f_y$ (referred to uncorroded specimens). Corroded specimens were submitted to the same load range as uncorroded ones, which was obtained by means of the uncorroded nominal diameter. In total 142 specimens were tested with ranging from 8% up to 28% degrees of corrosion. The pit observed in the failure cross-section of the reinforcement steel bar was characterized describing the pit geometry (pit depth and length) using a Vernier calliper. Further information regarding the experimental work is described by Fernandez et al.[21].

Due to the reduced existing database of corroded specimens submitted to high-cycle loading, half of the above-mentioned popultaion was employed for calibration purposes and the other half for the model validation. The σ-ε corroded properties were validated by means of different experimental studies [5,6,8,9,17,22].

4.4 Calibration of the critical pit parameters

Model calibration consisted in the definition of the pit in the critical cross-section, which resulted in the same experimental fatigue life value. Different geometrical pit parameters were tested until a good agreement between the experimental measured pit and the model pit was obtained, see Figure 10.

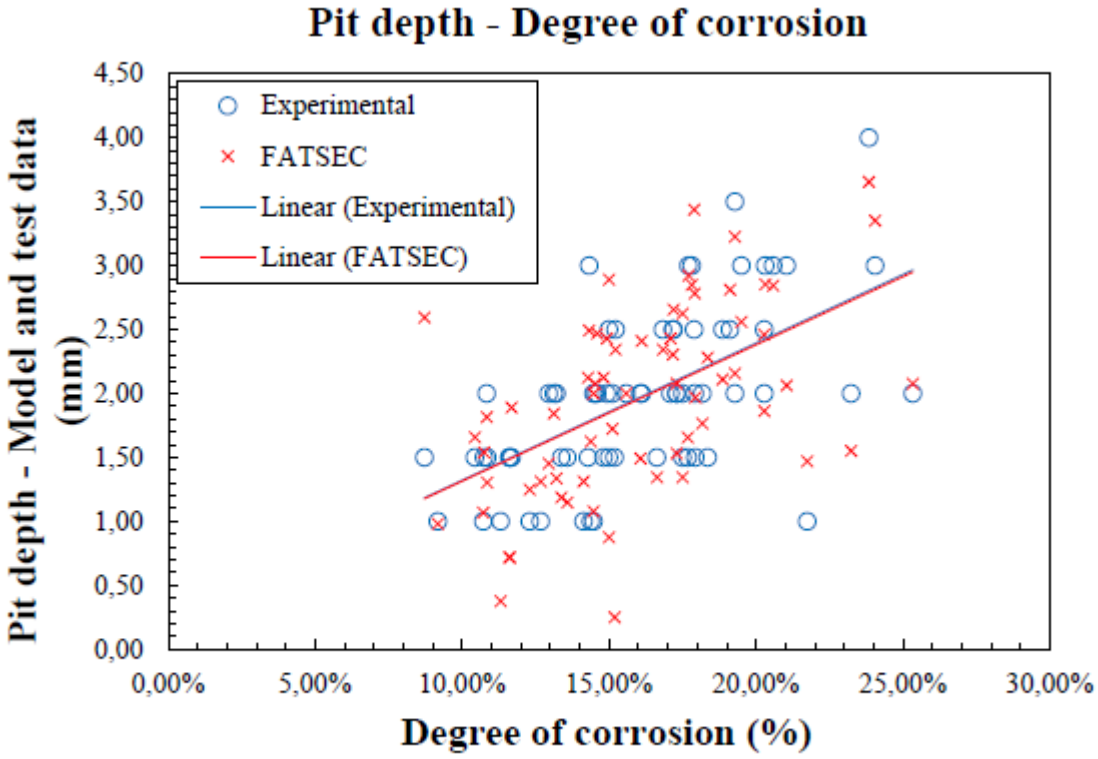

Figure 10. Pit depth-degree of corrosion. Experimental data and calibrated numerical model

A bisectional iterative algorithm was performed, which applied different notch geometries until the convergence was reached (the same resisted number of cycles). Critical pit length and depth were compared. The defined pit angle aperture, strongly conditioned the model pit depth, so different angle aperture relationships with respect to the degree of corrosion were tested to adjust this last parameter.

A dimensionless expression, eq (6), to describe the pit geometry characteristics with respect to the generalized corrosion was obtained from the model data. It was defined by the coefficient p/r_c (pit depth (p) and the resulting corroded radius (r_c), see Figure 7) and the steel bar degree of corrosion (generalized corrosion, g). Figure 11 shows the aforementioned obtained relationship. As it is described by Fernandez et al. [21] pit depth has major influence in the variations of the corroded steel mechanical properties, so it was chose to establish the relationship with the estimated degree of corrosion.

(6) $\frac{p}{r_c} = 2.318 \cdot g$ or $\frac{p}{\emptyset_c} = 1.159 \cdot g$

A log-Normal distribution adjusted very well to the obtained data and the experimental data, see Figure 12. The parameters of such distribution were mean=1.054, variance=0.092, mu=0.0134 and sigma=0.282.

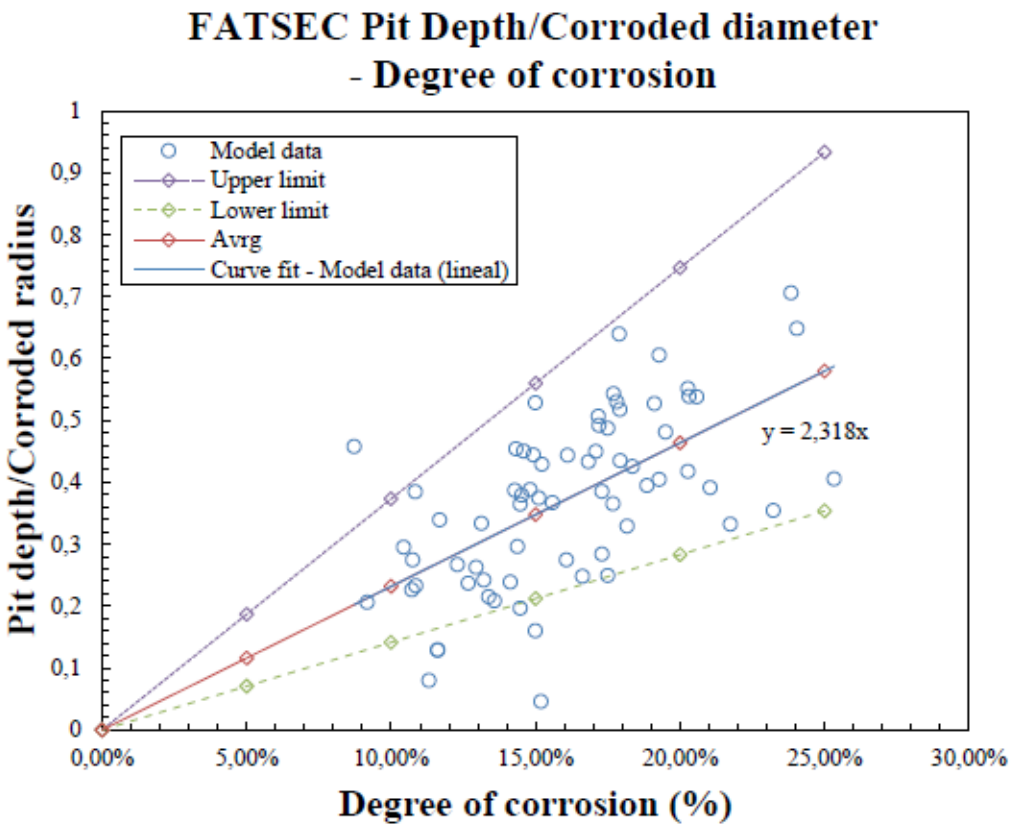

Figure 11. Relationship between degree of corrosion and the quotient pit depth - corroded bar diameter.

Upper and lower limits defined by the statistical model

The pit depth values for 0.95 and 0.05 quantiles could be obtained multiplying the average depth value got from (6) by 1.62 and 0.61 respectively. Therefore, the upper and lower bounds were defined; see Figure 11 and Figure 12.

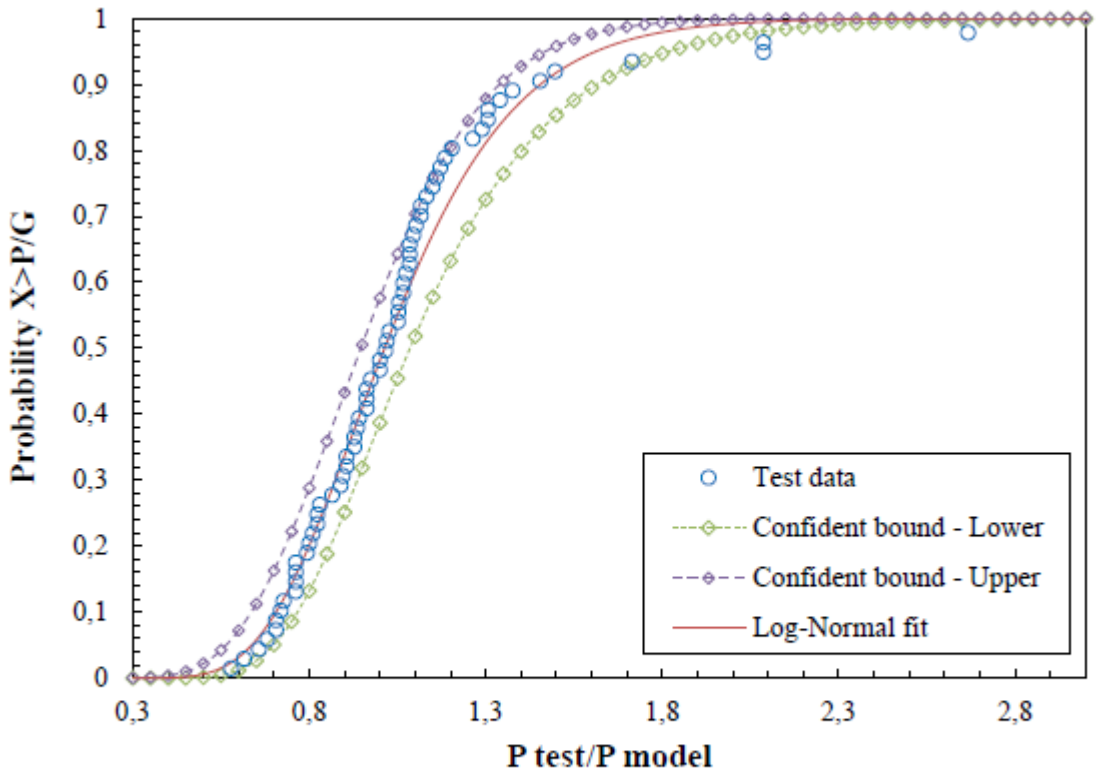

Figure 12. Statistical distribution of the pit depth and the log-Normal adjustment

296

297 *4.5 Pit characteristics sensitivity, depth, length and angle influence*

298 A sensitivity study of the principal variables that defined the idealized pit shape was performed.

299 4.5.1 Pit angle and pit depth

300 The pit depth was indirectly defined by the pit angle, so the pit angle determined the pit depth
301 model sensibility. Different pit angle apertures with respect to the degree of corrosion were
302 defined to observe their influence on the corroded steel tensile properties. Fixed and variable
303 angle apertures relationship were tested. In all the cases, the same value for the pit length was
304 used.

Figure 13a, Figure 13b, Figure 13c, and Figure 13d, represent the evolution of the main tensile monotonic parameters, yielding stress, ultimate stress, modulus of elasticity and maximum strain with respect to the degree of corrosion. Modulus of elasticity, yield stress and ultimate stress presented no significant variation with respect the different angle apertures used. However, higher degrees of corrosion presented higher differences. Nevertheless, the differences between the various angle apertures used were less than 5%. Strains showed a slightly higher scatter behaviour. Such behaviour was attributed to the higher impact of the amount of steel area reduction due to pitting than to the impact of the pit's shape, when it is referred to the tensile mechanical properties.

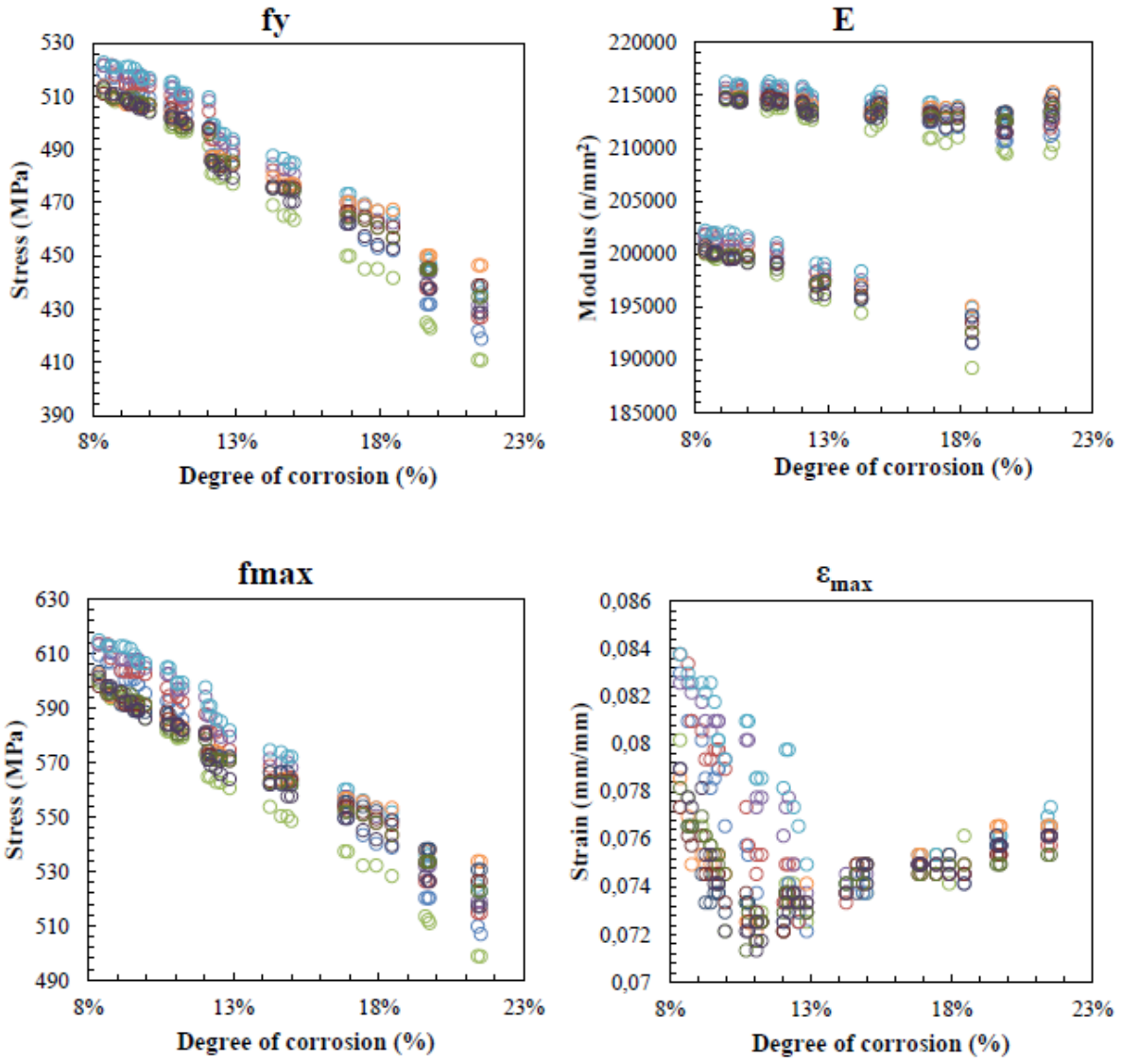

Figure 13. Corroded steel tensile properties – Pit angle variation. Each colour represents one different angle aperture with fixed length hypothesis

314

315 4.5.2 Pit length

316 The same analysis was performed to study the pit length sensitivity. Figure 14a, Figure 14b,
317 Figure 14c and Figure 14d, shows the evolution of the same parameters depicted in Figure 13,
318 using different pit length. The same pit angle was used in all cases. Four different length

hypotheses were made in order to test its influence on those parameters. The relationship between the pit length and the degree of corrosion almost did not affect the obtained results.

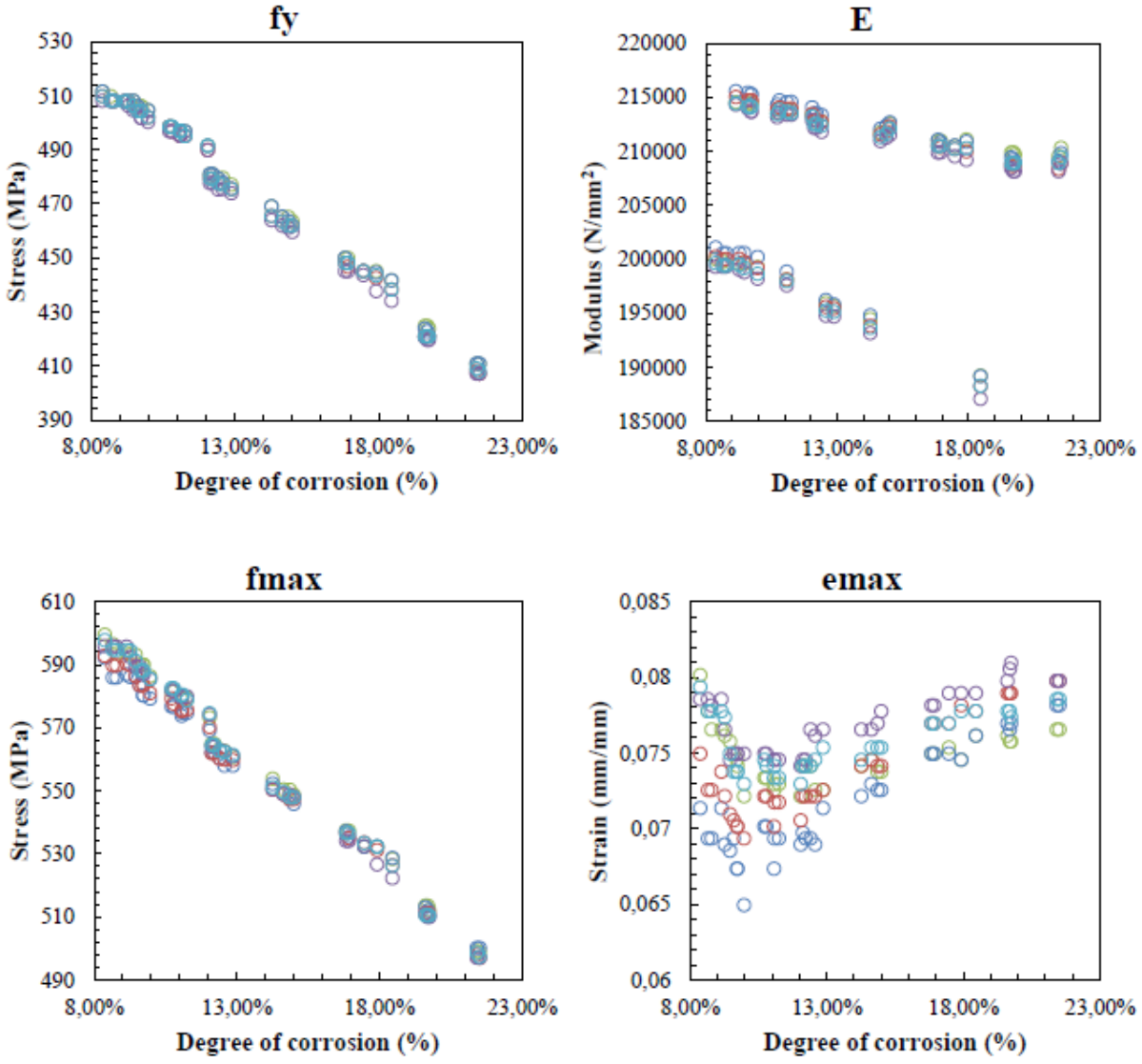

Figure 14. Corroded steel tensile mechanical properties - Pit length variation. Each colour represents one different pit length/corrosion level relationship with fixed angle hypothesis

4.5.3 Implemented pit geometry relationships

Finally, the implemented pit geometry characteristics regarding the degree of corrosion are shown in Figure 15 for 12 mm steel bar diameter.

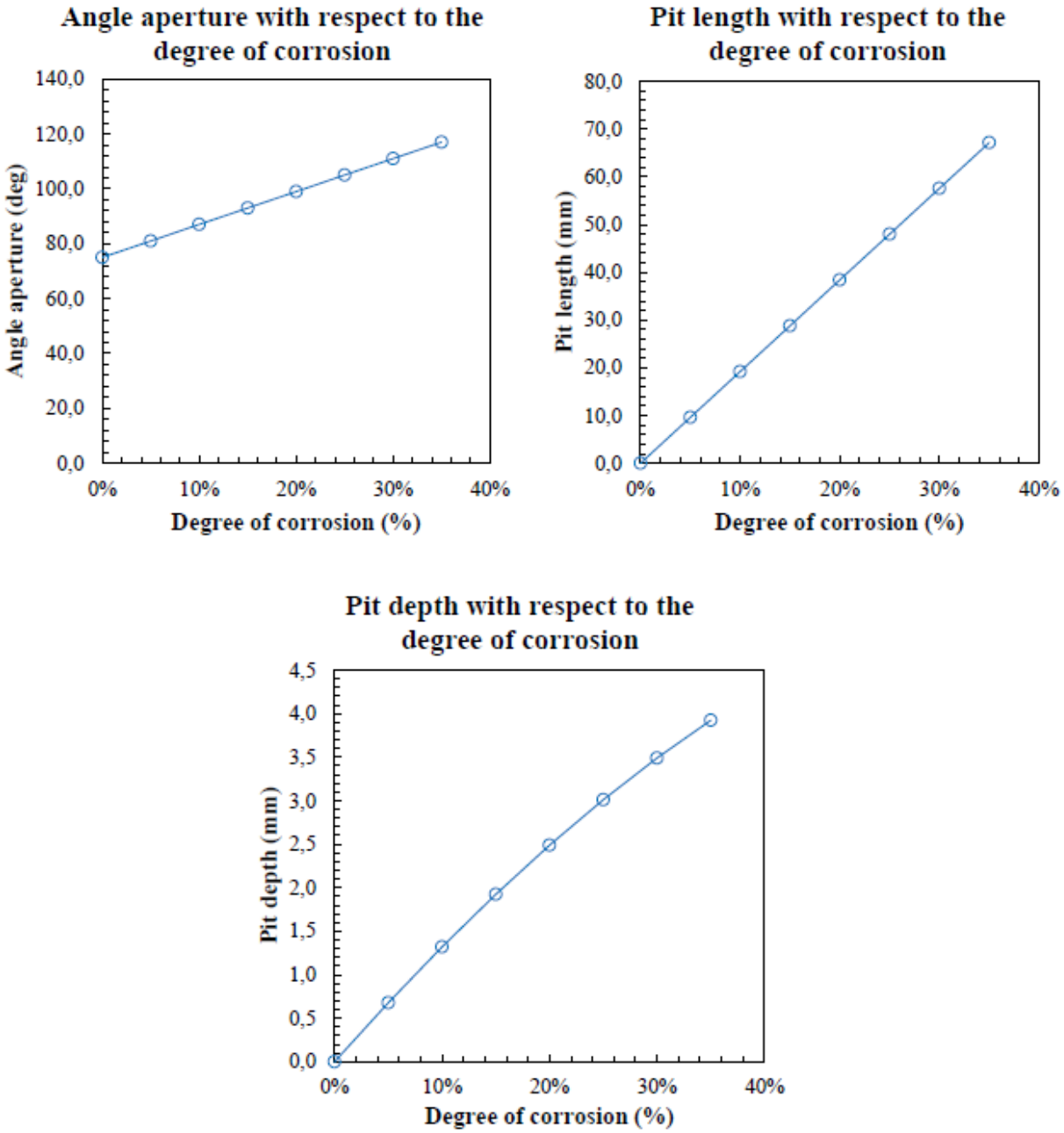

Figure 15. Pit geometry implementation for 12 mm diameter steel bar

According to the relationships described in Figure 15, the critical pitted cross-section was defined, and the notch performed. The different cross-section meshes that resulted after the application of the above criteria are represented in Figure 16.

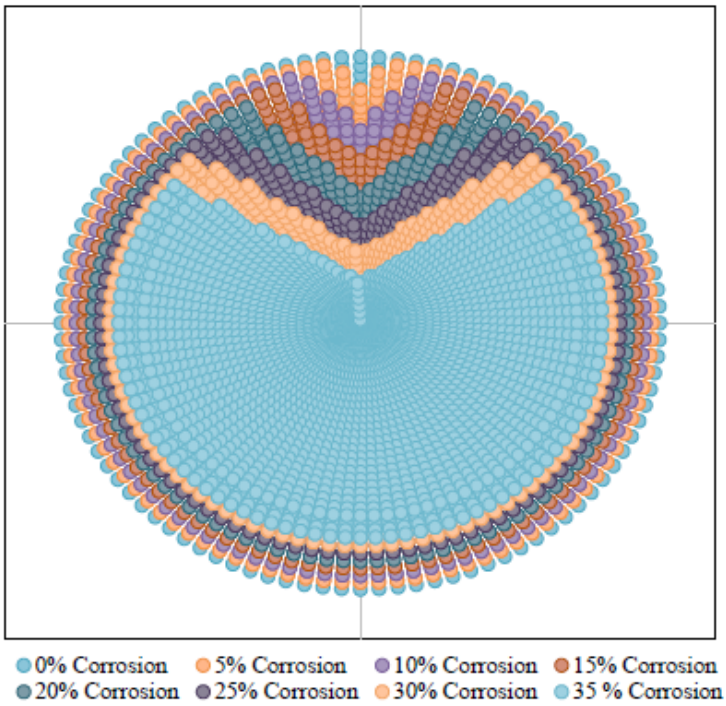

Figure 16. Mechanical model meshes for different degrees of corrosion (generalized corrosion with idealised critical pit)

5. S-N and σ-ε curves obtained from the calibrated mechanical model

The evolution of the corroded mechanical properties with respect to the degree of corrosion are presented in the next figures. The values expressed in the figures were obtained using the 95% percentile of the statistical model presented before for the pit depth. That percentile represented the most damage to the bar using deeper pit depths. Figure 17 and Figure 18 depicted the S-N and σ-ε curves for degree of corrosion between 5% up to 35%. The stress range represented in Figure

17 were referred to the nominal area of the uncorroded bar, as it was done in the experimental work [21]. However, depicted stresses in Figure 18 were referred to the generalized corroded area, without take into account the pit. This allows describing the σ-ε behaviour considering the estimated generalised corrosion of the bar.

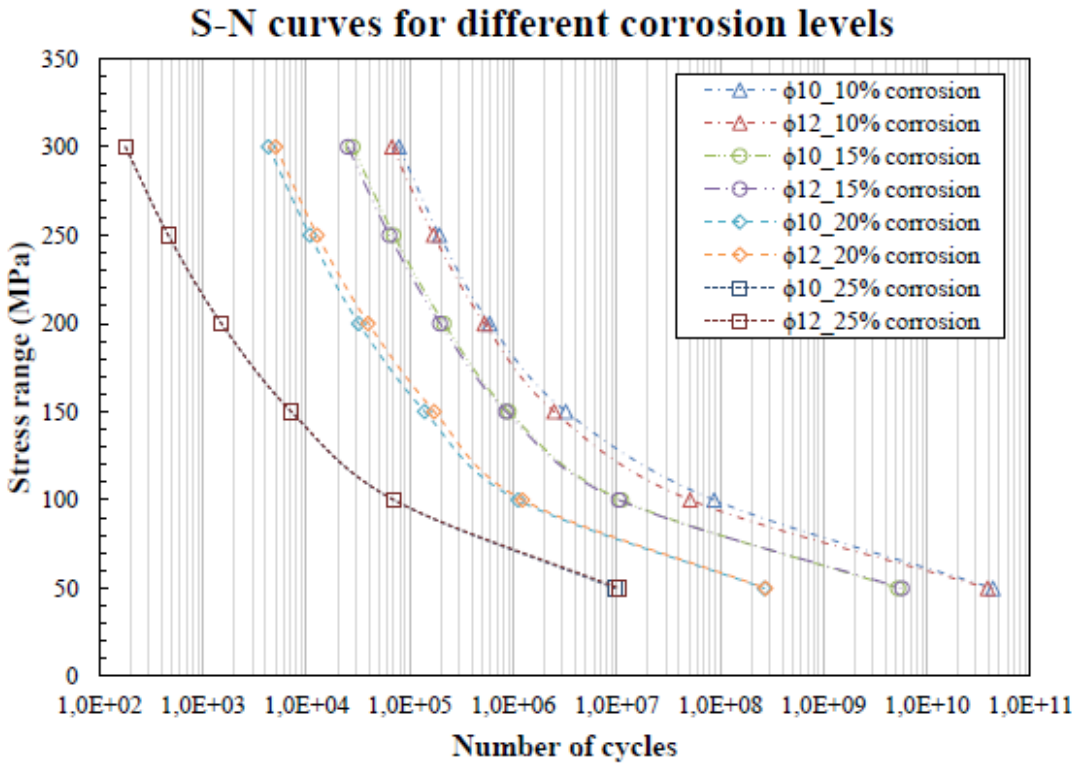

Figure 17. Fatigue curves obtained with the presented model for different degrees of corrosion and two diameters according to 95% characteristic pit – Stress range referred to nominal diameter

Few conclusions are remarkable from the presented results. The diameter effect (10 mm and 12 mm diameter) is not as relevant as the degree of corrosion impact in the fatigue life reduction. Fatigue strength is gradually reduced with respect to the degree of corrosion. However, the fatigue limit was maintained constant at 30 MPa indistinctly the degree of corrosion was, at least up to 25% degree of corrosion, which is a very high value.

346 An important reduction of the tensile mechanical properties described in the σ-ε curves presented
347 was obtained. As it is possible to observe the parameters represented did not describe a linear
348 reduction with respect to the degree of corrosion, behaviour already reported by Fernandez et al.
349 [21].

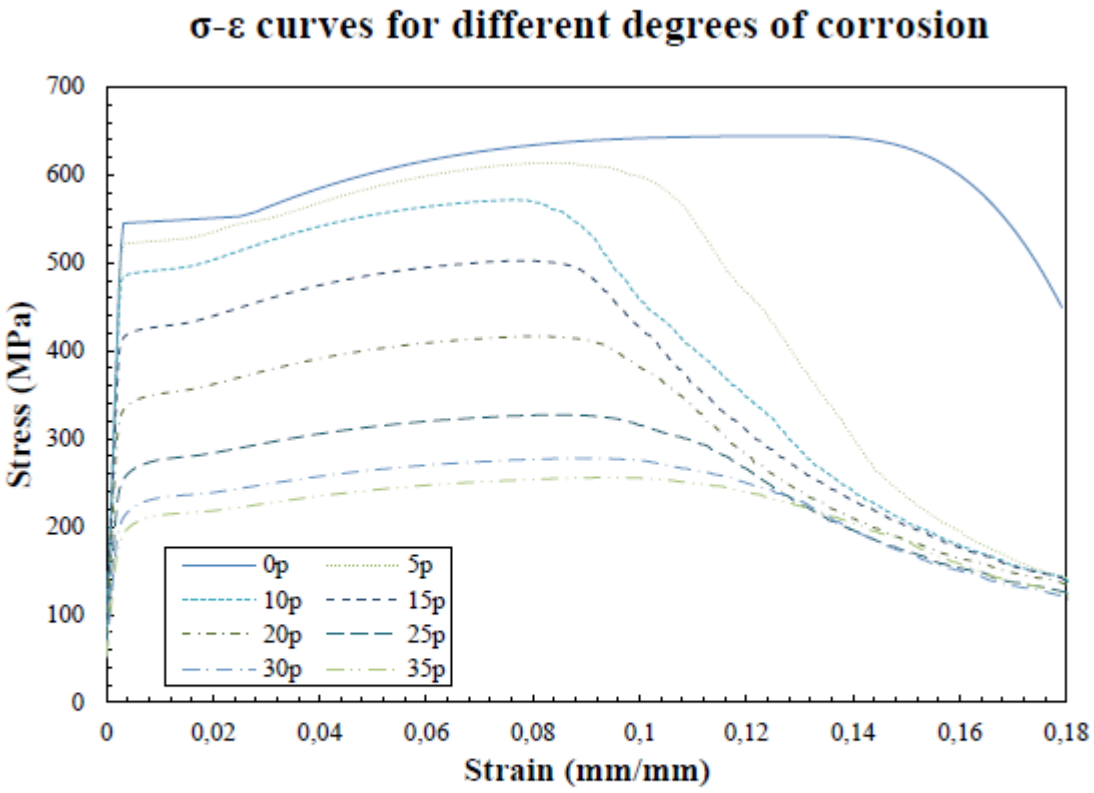

Figure 18. σ-ε curves obtained with the model for different degrees of corrosion according to 95% characteristic pit depth – Stresses referred to generalized degree of corrosion

350

351 **5.1 Model outputs**

352 5.1.2 Pit depth effect

353 In Figure 19 is described the effect of the pit depth for two different corrosion degrees, 10% and
354 35%, in terms of stress concentration effect around the pit. The distribution of the stress

355 concentration coefficient K1 from the tip of the pit to the surroundings of itself on the steel bar
356 cross-section is described. The stress amplification in the tip is around 25% in both cases;
357 however, 35% of corrosion degree steel bar showed much more penetration throughout the cross-
358 section than the lower corrosion degree.

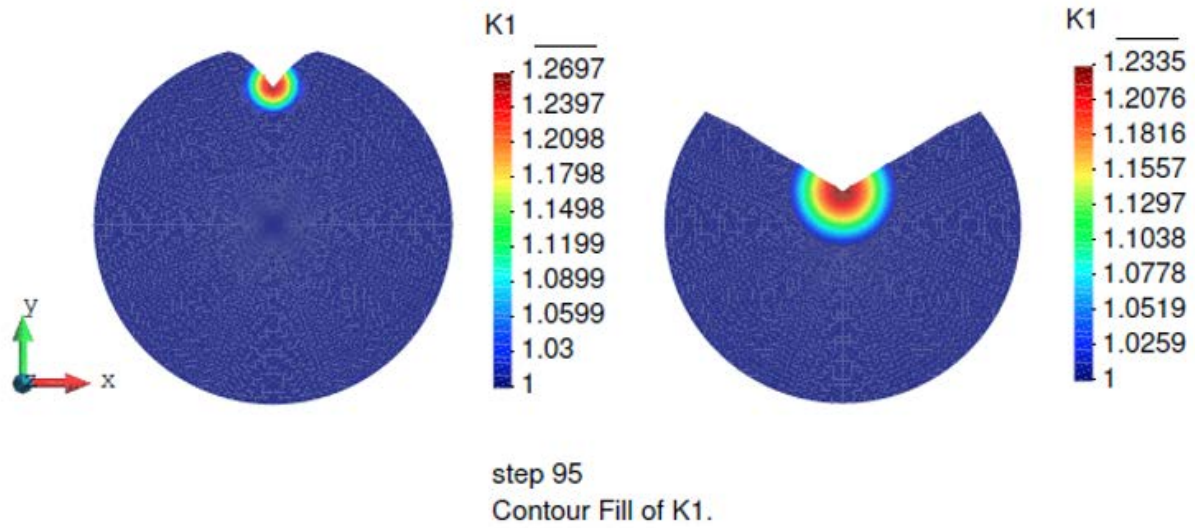

Figure 19. Stress concentration factor K1

359

360 5.1.2 Strain-stress state

361 The actual stress-strain state of two different cross-sections for a specific applied deformation are
362 showed in Figure 20. In both cases the applied deformation corresponded to ε=0.1178. The axial
363 load applied to fulfil with the aforementioned applied deformation was N=38.19 kN for 10%
364 corrosion degree whilst for 35% corrosion degree was N=19.26 kN. The actual stress as well as
365 the strain distribution due to the applied load are described. It is observed a higher amount of
366 compressed fibres with larger compression stresses 35% of corrosion degree, which was expected
367 due to the extra local bending induced by the high pit penetration along the cross-section (see
368 Supplementary Video 1 for full loading steps up to specimen failure description).

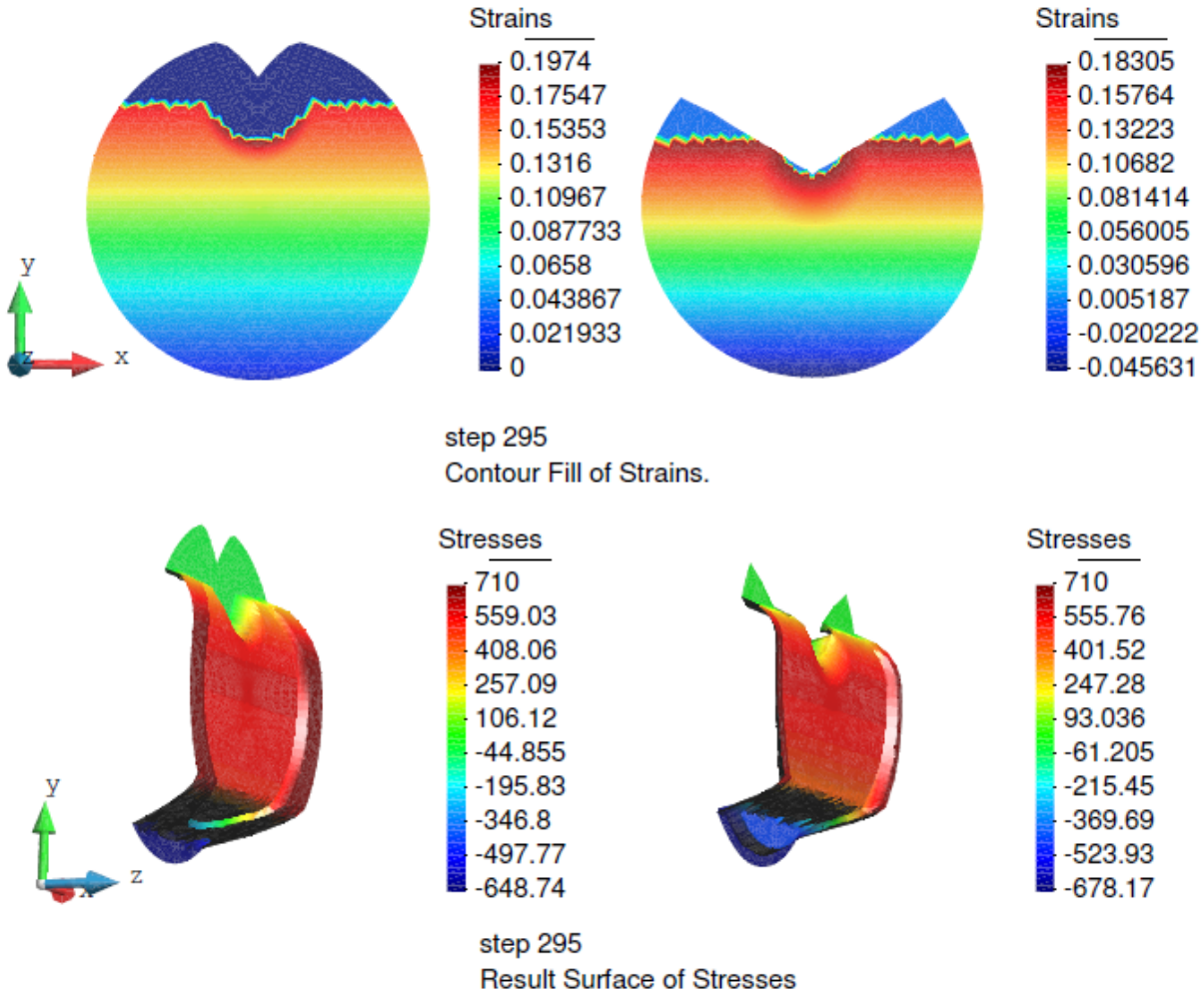

Figure 20. Strain-stress state.Step number 295, strain=0.1178

6. Model validation

6.1 Fatigue validation

Validation of the model for fatigue results was made using the other half of the availed population above described. Sixty-six specimens were used for validation purposes. The validation of the model consisted in the comparison of fatigue life value (number of resisted cycles) obtained from the test with respect to the achieved with the model, see Figure 21. As it is

possible to observe in the figure the data were well distributed along the line with slope 1, which means that the model thrown similar values to experimental data.

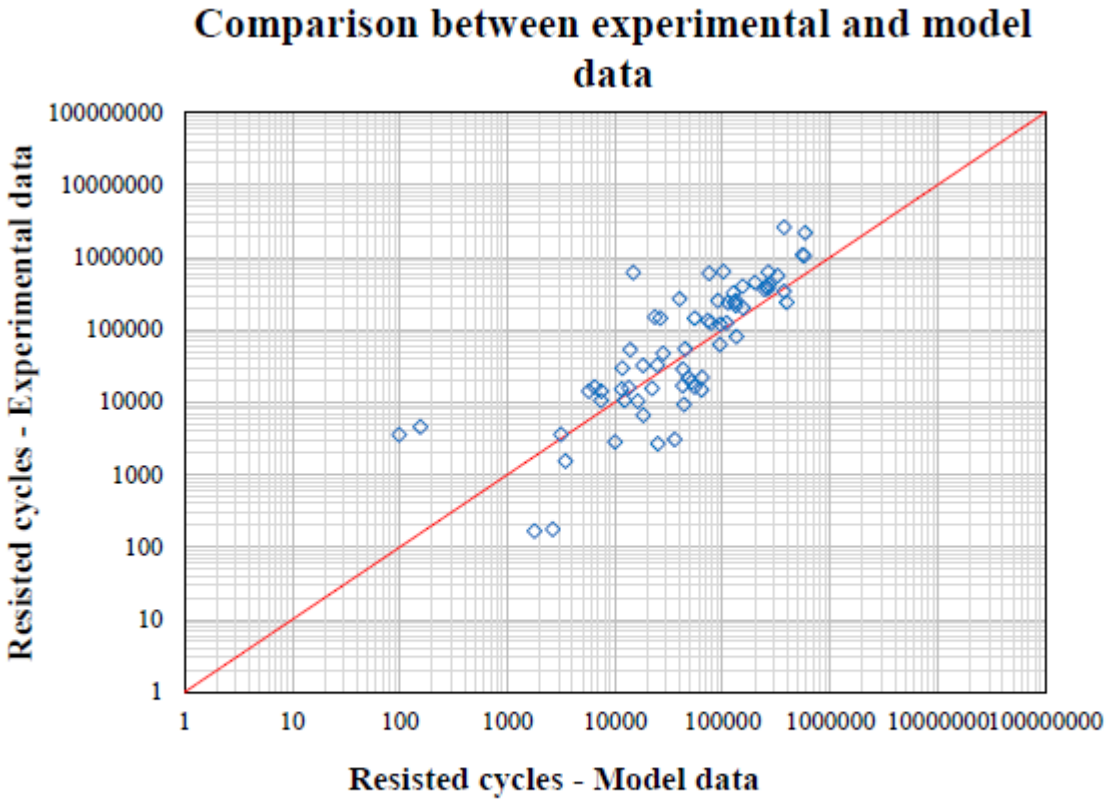

Figure 21. Fatigue validation for corroded specimens

In Figure 22, experimental and model data is compared. The pit depth characteristics upper and lower bound limits defined with the statistical model are also represented. All the tested stress range results were localized between the defined bounds. Taking into account the inner scatter behaviour of fatigue very good agreement was observed for the corroded steel fatigue life value estimation. It has to be noticed that for 150 MPa of stress range, the observed behaviour showed higher scatter than the other tested stress ranges. More data would be required to perform a better validation of the model for such low stress ranges.

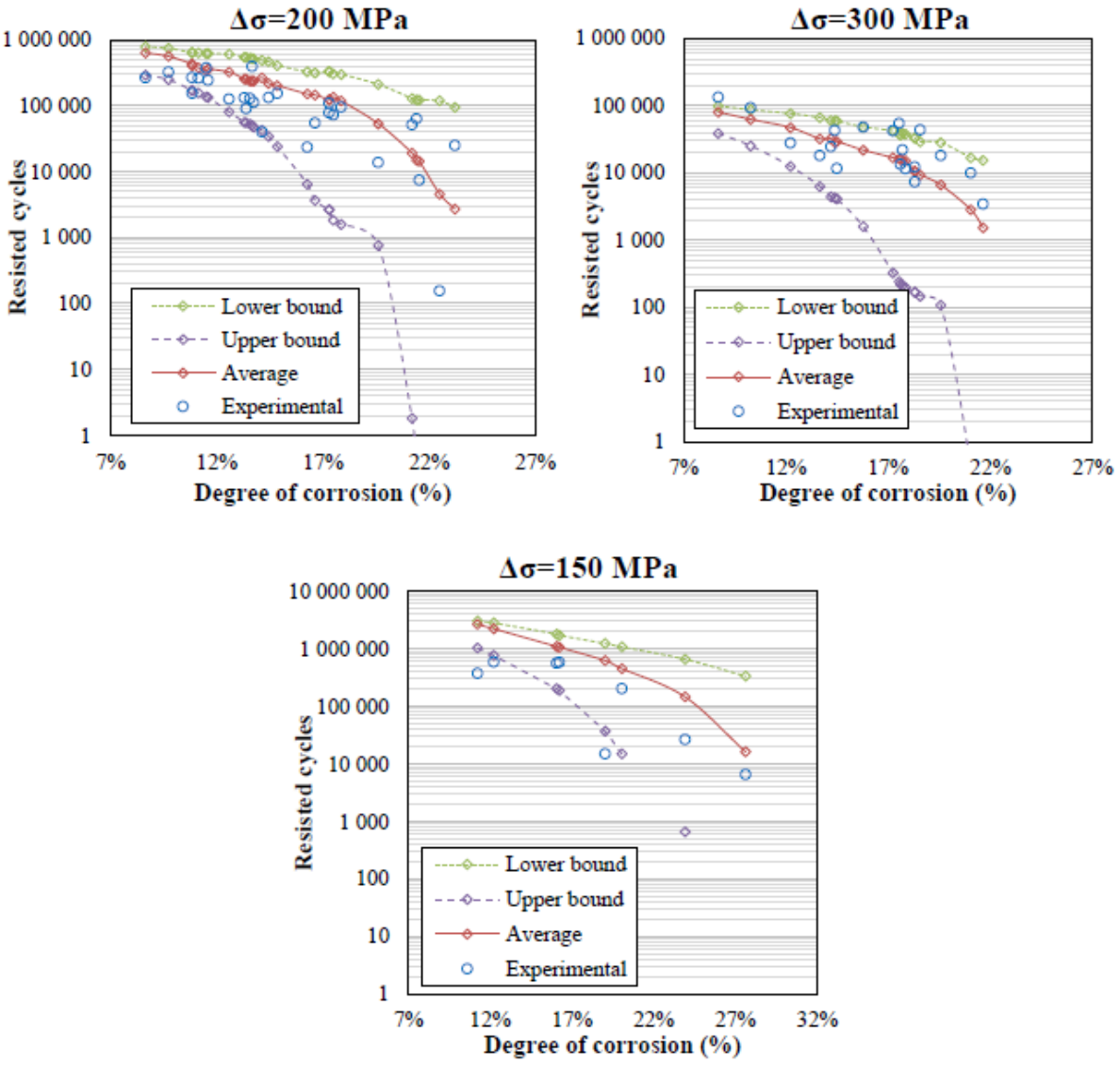

Figure 22. Fatigue validation. Model and experimental curves for the tested stress range

386

387 *6.2 Monotonic validation*

388 Four different sets of experimental data were taken for the corroded steel tensile properties
389 validation. Set one consisted of 25 specimens, which include a wide range of corroded specimens
390 from very little degrees of corrosion about 2% up to very high degrees of corrosion 60%. The

second set of bars encompassed 23 specimens covering a closer range of degrees of corrosion from 3% up to 16% [8]. The third set of specimens included 21 specimens also covering a full range of degrees of corrosion from 1% to 50% [22]. Finally the most extended database of specimens, which includes 54 specimens with two different bar diameter, ϕ10 mm and ϕ12 mm, and covering corrosions levels from 7% up to 25% [21]. The results of the model validations are presented in Figure 23, Figure 24, Figure 25 and Figure 26, in which are shown the experimental f_y or f_{max} compared to the model results, which include the upper and lower bounds.

Experimental and numerical data described very good agreement for yielding and ultimate stresses. Almost all the experimental data were localized in between the confident bounds defined with the presented statistical model. However, modulus of elasticity and maximum strain estimations were not as accuracy as yielding stress and ultimate stress ones. It is necessary to underline that the elastic modulus was obtained directly from the monotonic test not using the code recommendations for this parameter; hence, it could present some dispersion. Regarding maximum strain, it is subjected to other phenomena such as fracture mechanics due to pits in the cross-section.

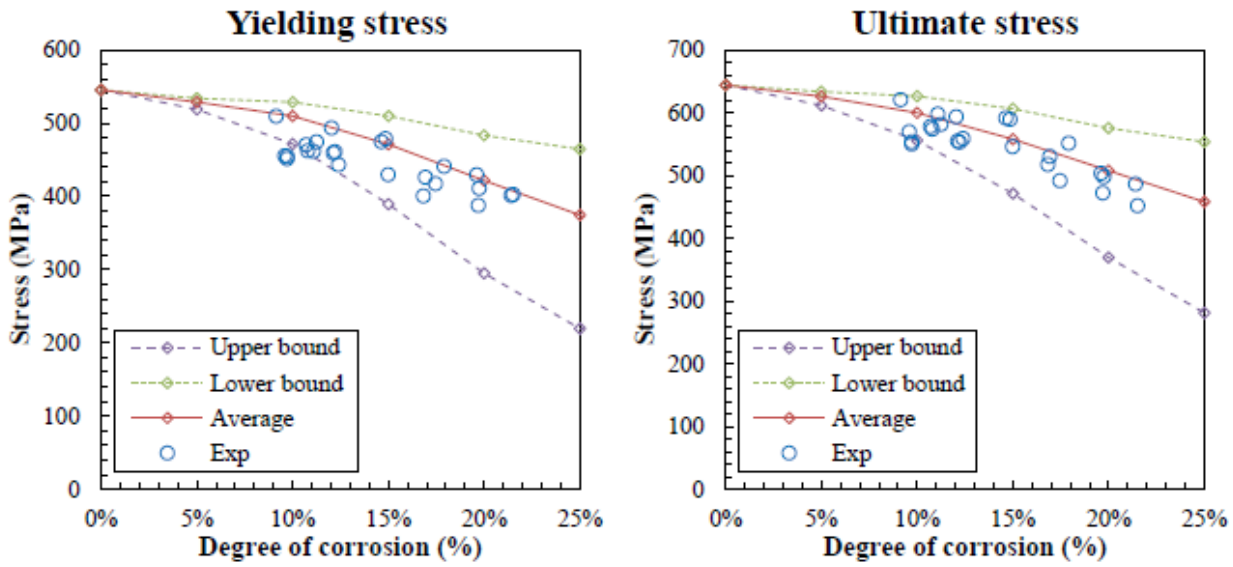

Figure 23. Monotonic validation. Fernandez et al. test [16]

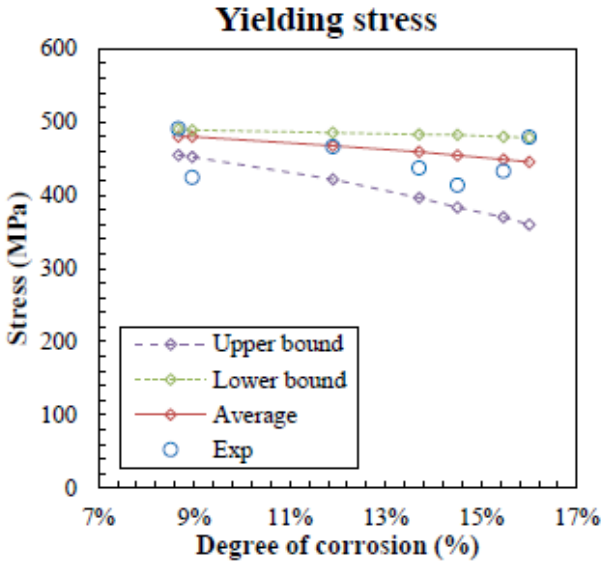

Figure 24. Monotonic validation. Apostolopoulos et al. test [19]

406

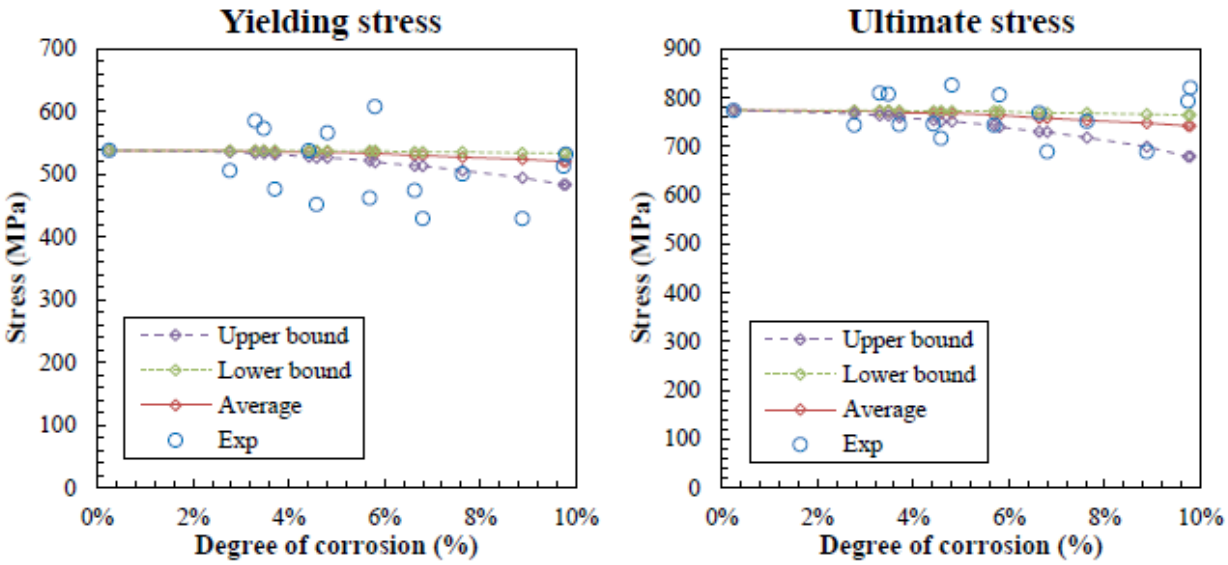

Figure 25. Monotonic validation. Apostolopoulos et al. test [19]

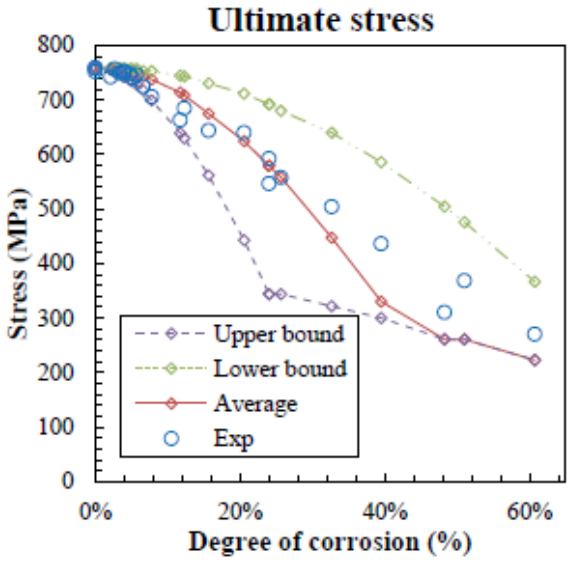

Figure 26. Monotonic validation. Abdullah A. et al. test [18]

407

7. Conclusions

A mechanical model to evaluate the effect of steel reinforcement corrosion on σ-ε and fatigue behaviour has been extended and presented. Corrosion phenomena has been implemented using an idealized pitted cross-section.

The main conclusions of the presented work are described in the next points:

- The experimental study showed a non-uniform distribution of the material properties throughout the steel cross-section. An increasing strength of the outer layers was observed, where the outer martensitic layer achieved up to 806 MPa yielding stress. The inner ferrite core achieved up to 435 MPa yielding stress. The effect of material properties distribution is stated as relevant during a corrosion episode.
- The statistical model presented define different pit geometries with respect to the expected corrosion level. That allows describing the upper and lower bound limits of the pit geometry characteristics, ensuring that the real mechanical properties of the corroded steel bar will be inside those bounds with a 90% of confident.
- Very good agreement was observed for yielding stress and ultimate stress within a 0% - 60% degree of corrosion. The model allows to describe quite well the average behaviour of the corroded bars mechanical properties despite the experimental scatter values. Elastic modulus and ductility presented more dispersion, likely because of the dispersion of these parameters themselves, and the model did not adjusted the average behaviour as well as for the other parameters. More detailed studies are needed to better calibrate the model response for those values.

- The mechanical model can describe the fatigue behaviour under corrosion phenomenon with a very good agreement with the experimental data. Then, the characteristic fatigue curves with respect to the degree of corrosion can be defined.

As a general conclusion, the model leads to a good mechanical properties characterization for corroded and uncorroded bars, necessary properties to carry out with enough accuracy analysis and assessment of safety, serviceability and durability of deteriorated reinforced concrete structures. However, more experimental work should be addressed to further calibrate and validate the presented model for Low Cycle Fatigue, which is of interest in seismic zones.

Acknowledgments

The authors wish to acknowledge the financial support of The Ministry of Economy and Competitiveness of the Government of Spain (MINECO) for providing funds for projects BIA2009-11764, BIA2012-36848 and the European Regional Development Funds (ERDF). The financial support of Infrastructures de Catalunya (ICAT) is also highly appreciated. Acknowledgements are also extended to CIMNE to providing a license of the software GiD necessary to develop the presented work.

References

[1] L. Bertolini, B. Elsener, P. Pedeferri, R. Polder, Corrosion of Steel in Concrete. Prevention, Diagnosis, Repair., Wiley-VCH Verlag GmbH & Co. KGaA, Weinheim, Germany, 2004.

[2] K. Tutti, Corrosion of steel in concrete, (1997) 6–15. doi:10.4324/9780203414606_chapter_2.

[3] J. Broomfield, Corrosion of steel in concrete: understanding, investigation and repair, 2nd Ed., Taylor & Francis, Abingdon, United Kingdom, 2002.

[4] M. Raupach, B. Elsener, R. Polder, J. Mietz, Corrosion of reinforcement in concrete, Woodhead Publishing Limited, 2007. doi:10.1533/9781845692285.

[5] W. Zhang, X. Song, X. Gu, S. Li, Tensile and fatigue behavior of corroded rebars, Constr. Build. Mater. 34 (2012) 409–417. doi:10.1016/j.conbuildmat.2012.02.071.

[6] C.A. Apostolopoulos, Mechanical behavior of corroded reinforcing steel bars S500s tempcore under low cycle fatigue, Constr. Build. Mater. 21 (2007) 1447–1456. doi:10.1016/j.conbuildmat.2006.07.008.

[7] C.A. Apostolopoulos, M.P. Papadopoulos, S.G. Pantelakis, Tensile behavior of corroded reinforcing steel bars BSt 500s, Constr. Build. Mater. 20 (2006) 782–789. doi:10.1016/j.conbuildmat.2005.01.065.

[8] C.A. a. Apostolopoulos, V.G.G. Papadakis, Consequences of steel corrosion on the ductility properties of reinforcement bar, Constr. Build. Mater. 22 (2008) 2316–2324. doi:10.1016/j.conbuildmat.2007.10.006.

[9] C.A. Apostolopoulos, S. Demis, V.G. Papadakis, Chloride-induced corrosion of steel reinforcement – Mechanical performance and pit depth analysis, Constr. Build. Mater. 38 (2013) 139–146. doi:10.1016/j.conbuildmat.2012.07.087.

[10] A. Apostolopoulos, T. Matikas, C. Apostolopoulos, G. Diamantogiannis, Pit Corrosion Examination of Bare and Embedded Steel Bar, in: Adv. Met. Mater. Technol., Saint Petersburg, 2013: pp. 489–495.

[11] F. Biondini, M. Vergani, Deteriorating beam finite element for nonlinear analysis of concrete structures under corrosion, Struct. Infrastruct. Eng. 11 (2014) 519–532. doi:10.1080/15732479.2014.951863.

[12] H. Çetinel, M. Toparlı, L. Özsoyeller, A finite element based prediction of the microstructural evolution of steels subjected to the Tempcore process, Mech. Mater. 32 (2000) 339–347. doi:10.1016/S0167-6636(00)00009-0.

[13] I. Sankar, K. Rao, A. Gopalakrishna, Optimization of steel bars subjected to Tempcore process using regression analysis and harmony search algorithm, J Sci Ind Res. 69 (2010) 266–270. http://nopr.niscair.res.in/handle/123456789/7713 (accessed July 10, 2014).

[14] J. Nikolaou, G.. Papadimitriou, Microstructures and mechanical properties after heating of reinforcing 500 MPa class weldable steels produced by various processes (Tempcore, microalloyed with vanadium and work-hardened), Constr. Build. Mater. 18 (2004) 243–

254. doi:10.1016/j.conbuildmat.2004.01.001.

[15] P. Simon, M. Economopoulos, P. Nilles, Tempcore: a new process for the production of high quality reinforcing bars, Iron Steel Eng. 61 (198AD) 55–67.

[16] J.M. Bairan, a. R. Marí, H. Ortega, J.C. Rosa, Effects of winding and straightening of medium and large diameter reinforcing bars manufactured in coils in their mechanical properties, Mater. Construcción. 61 (2011) 559–581. doi:10.3989/mc.2011.60110.

[17] C.A. Apostolopoulos, G. Diamantogiannis, A.C. Apostolopoulos, Assessment of the Mechanical Behavior in Dual-Phase Steel B 400 C , B 450 C , and B 500 B in a Marine Environment, 28 (2016) 1–9. doi:10.1061/(ASCE)MT.1943-5533.0001271.

[18] A. Dimatteo, M. Vannucci, V. Colla, A Finite Element Method for the Prediction of Thermal, Metallurgical, and Mechanical Behavior of Rebars in the TempCore Process, Steel Res. Int. 87 (2016) 276–287. doi:10.1002/srin.201500029.

[19] A.G. Palmgren, Die Lebensdauer von Kugellagern (life length of roller bearings), VDI Z. 68 (1924) 339–341.

[20] M.A. Miner, Cumulative damage in fatigue, J. Appl. Mech. 12 (1945) A159–A164.

[21] I. Fernandez, J.M. Bairán, A.R. Marí, Corrosion effects on the mechanical properties of reinforcing steel bars. Fatigue and σ–ε behavior, Constr. Build. Mater. 101 (2015) 772–783. doi:10.1016/j.conbuildmat.2015.10.139.

[22] A. a. Almusallam, Effect of degree of corrosion on the properties of reinforcing steel bars, Constr. Build. Mater. 15 (2001) 361–368. doi:10.1016/S0950-0618(01)00009-5.

[23] UNE-EN-ISO-15630-01, Steel for reinforced and prestresed concrete - Testing methods. Part 1: Bars and wires for reinforced concrete, (n.d.).

[24] A. Borruto, Meccanica della frattura, Milan, 2002.

[25] I. Fernandez, M.F. Herrador, A.R. Marí, J.M. Bairán, Structural effects of steel reinforcement corrosion on statically indeterminate reinforced concrete members, Mater. Struct. (2016). doi:10.1617/s11527-016-0836-2.

[26] C. Alonso, C. Andrade, J. Rodriguez, J.M. Diez, Factors controlling cracking of concrete affected by reinforcement corrosion, Mater. Struct. 31 (1998) 435–441. doi:10.1007/BF02480466.

[27] C. Andrade, C. Alonso, F.J. Molina, Cover cracking as a function of bar corrosion: Part I-Experimental test, Mater. Struct. 26 (1993) 453–464. doi:10.1007/BF02472805.

[28] Y. Ballim, J.C. Reid, Reinforcement corrosion and the deflection of RC beams - An experimental critique of current test methods, Cem. Concr. Compos. 25 (2003) 625–632. doi:10.1016/S0958-9465(02)00076-8.

[29] A.K. Azad, S. Ahmad, S.A. Azher, Residual Strength of Corrosion-Damaged Reinforced Concrete Beams, ACI Mater. J. 104 (2007) 40–47. http://0-proquest.umi.com.library.newcastle.edu.au:80/pqdweb?did=1208508371&Fmt=7&clientId=29744&RQT=309&VName=PQD.

[30] R. Huang, C.C. Yang, Condition assessment of reinforced concrete beams relative to

reinforcement corrosion, Cem. Concr. Compos. 19 (1997) 131–137.

[31] T.E.A. El Maaddawy, K.K.A. Soudki, Effectiveness of impressed current technique to simulate corrosion of steel reinforcement in concrete, J. Mater. Civ. …. (2003) 41–47. http://ascelibrary.org/doi/abs/10.1061/(ASCE)0899-1561(2003)15:1(41) (accessed July 3, 2014).

[32] M. Badawi, K. Soudki, Control of Corrosion-Induced Damage in Reinforced Concrete Beams Using Carbon Fiber-Reinforced Polymer Laminates, J. Compos. Constr. 9 (2005) 195–201. doi:10.1061/(ASCE)1090-0268(2005)9:2(195).

[33] ASTM Standard G1, Standard practice for preparing, cleaning, and evaluating corrosion test specimens, (2011).